# Theoretical and experimental analysis of circularly polarized luminescence spectrophotometers for artifact-free measurements using a single CCD camera.

**bruno baguenard**
Université Lyon 1
**amina Bensalah-Ledoux**
Université Lyon 1 https://orcid.org/0000-0003-3016-2994
**Laure Guy**
ENS Lyon https://orcid.org/0000-0002-8728-7213
**François Riobé**
Univ Lyon, Ens de Lyon, CNRS UMR 5182, Université Claude Bernard Lyon 1 https://orcid.org/0000-0001-6746-8132
**Olivier Maury**
**Stephan Guy** ( stephan.guy@univ-lyon1.fr )
Université Lyon 1 https://orcid.org/0000-0003-2145-0097

**Article**

**Keywords:**

**Posted Date:** July 1st, 2022

**DOI:** https://doi.org/10.21203/rs.3.rs-1722896/v1

# Theoretical and experimental analysis of circularly polarized luminescence spectrophotometers for artifact-free measurements using a single CCD camera.

June 13, 2022

**Abstract**

We demonstrate the feasibility of artifact-free measurements of Circularly Polarised Luminescence (CPL) spectra on an imaging spectrometer. The polarization is spatially separated on two measurement channels using an achromatic quarter-wave plate associated with a polarizing beam splitter. The two channels are then imaged on a spectrometer to give the left and right circularly polarized spectra. The artifacts have been highlighted via the Mueller formalism and verified experimentally. As they add spectral contributions from either the shape of the luminescence or its derivative, they are almost impossible to eliminate by pre-calibration. We show that, at the cost of a second measurement that reverses the role of the two measuring arms, these artifacts are reduced in proportion to the stability of the lamp. The experimental results show the ability of our setup to measure CPL spectra on different kind of molecules in an accurate way with a dramatic (3 orders of magnitude) reduction in the recording time compared to a standard step by step measurement.

The interactions between circularly polarized light and chiral material are unequal for left-handed and right-handed circular polarizations and are revealed by different phenomena such as optical rotation (refractive index difference) , electronic circular dicroism (ECD) (UV-VIS absorption difference), vibrational VCD (IR absorption difference) and so on [1]. The luminescence from chiral luminophore is also asymmetric in term of handedness which lead to the Circular Polarized Luminescence CPL= $\Delta I = I_{\mathrm{L}} - I_{\mathrm{R}}$ corresponding to the difference between the left handed circular polarization (LHCP) and the right handed circular polarization (RHCP) luminescence [2]. CPL spectra of the enantiomers are opposite and the intensity of the signal is quantified by the dissymmetry factor $g_{lum} = 2(I_{\mathrm{L}} - I_{\mathrm{R}})/(I_{\mathrm{L}} + I_{\mathrm{R}})$. $g_{lum}$ is of the order of $10^{-3}$ to $10^{-5}$ for most organic molecules [3, 4]. CPL is a valuable complementary tool to the more standard ECD spectroscopy because it allows to access different electronic transitions and can be detected in non-transparent media [5, 6]. During the last years, we observe a craze for CPL because of the synthesis of molecules or chiral systems with $g_{lum}$ higher than $10^{-3}$ making CPL a valuable alternative for the detection of chiral environmental probes or to conceive devices producing circularly polarized light [6, 7, 8, 9, 10, 11, 12, 13]. Thus, the need for reliable, robust and fast CPL measurements is becoming crucial.

Most of the CPL spectrometers are based on a polarization modulation scheme: the polarization is modulated between the two LHCP and RHCP at some tens of KHz frequency with a photo-elastic modulator (PEM) [2]. The Fourier analysis of the signal allows to get the excess of circular polarization. The limit of detection is determined by the integration time of the lock-in amplifier used to demodulate the signal. This system requires a fast mono-channel detector (photo-multiplier or photodiode) with a time constant lower than the modulation period (20µs for common PEM). Thus, it prevents the use of CCD camera which have, generally, millisecond long integration times. The spectra are necessarily recorded step by step and the recording times may last several tens of minutes making this technique very heavy and limited to fundamental studies. This technique has proven its efficiency with measured spectra of $g_{lum} \leq 10^{-4}$ and its validity and related artifacts have been well investigated [14].

In this work, we investigate the use of a CCD camera for a fast recording of full CPL spectra. Because, high speed modulation can not be used (except for non commercially available specialized camera [15]), CCD based spectra must rely on a spatial polarization separation scheme. Spatial beams polarization splitting is

| Defect | Origin | Parameter | magnitude |
|---|---|---|---|
| QWP retardance $\Psi \neq \frac{\pi}{2}$ | QWP specifications - chromaticity | $\psi = \Psi - \frac{\pi}{2}$ | $\pm\frac{\pi}{50}$ over 500nm |
| QWP azimuth $\theta \neq \pm\frac{\pi}{4}$ | Mis-alignement | $\alpha = \theta - \frac{\pi}{4}$ | $\pm\frac{\pi}{200}$ |
| Unequal arms transmission: $T_{+1} \neq T_{-1}$ | PBS, fibers, grating | $\Delta T = \frac{T_{+1}-T_{-1}}{T_{+1}+T_{-1}}$ | $10^{-2}$ |
| Polarization mixing | imperfect exctinction ratio (PBS), straylight | $\varepsilon_p,\ \varepsilon_s,\ \sigma_l$ | $10^{-2}$-$10^{-3}$ |
| Pump source variations: $\phi_{+1} \neq \phi_{-1}$ | LED stability | $\Delta\phi = \frac{\phi_{+1}-\phi_{-1}}{\phi_{+1}+\phi_{-1}}$ | $10^{-2}$-$10^{-3}$ |
| Wavelength mismatch: $\lambda_{+1} \neq \lambda_{-1}$ | monochromator misalignement | $\Delta\lambda = \frac{\lambda_{+1}-\lambda_{-1}}{2}$ | 0.1nm |

**Table 1:** The different defects of the setup limiting the experimental measurements, their origin, the parameters describing them and their magnitudes.

commonly used for full polarization characterization, i.e Mueller imaging. It is generally dedicated to single wavelength and/or high polarization dissymmetry ($\geq 10^{-2}$) phenomenon measurements, as complex procedures are required to calibrate each of the optical elements [16]. For measuring subtle spectral chiroptical signals, use of CCD camera after polarization beam splitting have been demonstrated for Raman optical activity [17] and CPL measurements [18, 19] and ourselves [20, 21]. The needed accuracy – of the order of 0.01% on the polarization difference – requires an equal control of the two analysis arms. This is almost impossible to achieve over the entire wavelength range and a very complex calibration procedure is proposed by Mackenzie [18]. Hug and Hangartner showed that by inverting the role of the two arms, the unequal arms transmission is auto-compensated [17]. Their setup was successfully commercialized by Biotools. On our side, we have also performed CPL measurements on a single camera by only separating the luminescence according to two polarization encoded optical paths [21]. However, even-though the use of only one camera reduces the artefacts sources, appropriate calibration procedure is still needed to avoid remaining defects and inaccurate signals recording.

In this study, we show that, at the cost of two successive measurements, corresponding to the swap of the two optical paths, and then their average, reliable spectra of CPL can be obtained. The performances and limitations of this method are fully investigated. The article is organized as follow. In the first part, after describing the experimental setup, we theoretically analyze the recorded spectra via the Mueller matrix framework. Three configurations are investigated: simultaneous measurements on two arms (spatial separation of polarization), successive measurements on one arm (time polarization's separation) and combination of the two previous ones (space-time combination of polarization's separation). First order calculations show that a first order false signal appears for spatial and time polarization's separations. These signals multiply together in the space-time combination and consequently the related artifacts become very low.

These theoretical finding are experimentally illustrated in the second part of the paper, on broad ($\sim$ 50 nm) and narrow line ($\sim$ 1 nm) spectra from camphorquinone and $Eu^{3+}$ complexes , respectively. Moreover, in order to assess the limits of our method and to verify its performance, we compare the spectra obtained with the camera to those obtained with our "home-made" single channel PEM based setup described elsewhere [7, 22, 23].

This work shows that CPL free from first order artifacts can be recorded in a few seconds over a wavelength range between 300 and 1050 nm with a multi-channel coverage of 150-300 nm depending on the grating and optical magnification. The only limitation is the analog to digital converter of the CCD which gives a limit of detection $g_{lum} \sim 5.10^{-4}$. This works opens perspectives on fast/automatic measurement of CPL in automated processes.

# 1 Optical set-up

## 1.1 Single CCD-based CPL apparatus

The home-made single CCD based CPL spectrometer is schematically represented in Figure 1. Basically, the handedness of the circularly polarized luminescence is spatially encoded into two geometrical paths before

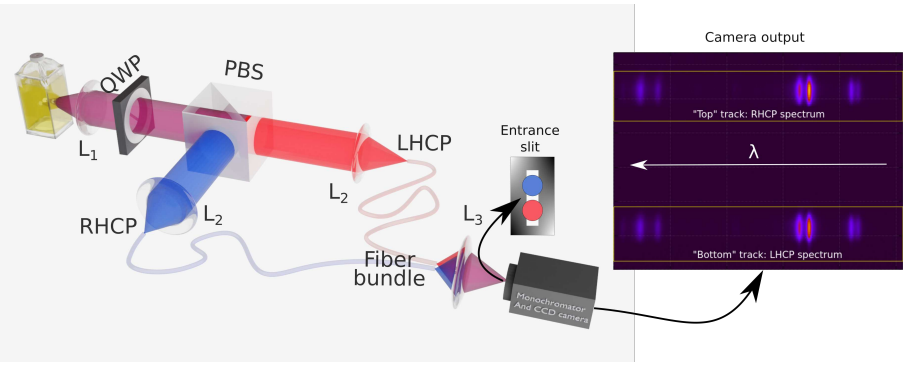


**Figure 1: Schematic of the CCD-based CPL spectrometer:** The fluorescence light is collected via lens $L_1$. After the quarter-waveplate (QWP, main axis 45°) and the polarizing beam spliter (PBS, main axis 0°) the LHCP and RHCP are transmitted and reflected respectively (as horizontally and vertically polarized light). The two beams are launched into two fibers with a lens $L_2$, for each arm. These two fibers merge as a bundle. The bundle output is imaged via lens $L_3$ as two vertically separated spots on the entrance slit of the monochromator (see SI, Sec 1). The two spots are horizontally diffracted by the gratting giving on the CCD camera the top/bottom spectrum coming from the top/bottom spots and thus related to the LHCP and RHCP emission. Here, the image is recorded from an $Eu^{3+}$ complex **2**.

being spectraly dispersed by the spectrometer and recorded on the CCD camera. This is accomplished by the association of a quarter wave plate (QWP, fast axis 45°) and a polarizing beam spliter (PBS): the left handed circularly polarized (LHCP) ligth is transmitted by the PBS (0° linear polarization) while the right handed circularly polarized (RHCP) ligth is reflected by the PBS (90° linear polarization). The two handedness-encoded beams are then routed at the adjustable entrance slit of the spectrometer by means of a dual core fiber bundle (200µm diameter). The two beams are spatially imaged as two vertically aligned spots on the entrance slit. Inside the spectrometer (see SI, Sec 1 for details), the input slit is imaged on the CCD camera (Andor iDus-420) after being horizontally diffracted by the grating leading to two vertically split spectra: the top (bottom) one corresponds to the top(bottom) fiber and consequently to the RHCP (LHCP) luminescence.

Using a single spectrophotometer with only one CCD array camera avoids stability issues between two detectors and reduces the price of the setup, by saving one spectrophotometer, as regard CPL setups based on two of theme [18, 19].

### 1.2 Three ways of measuring CPL

Here we experimentally investigate CPL recording using time, spatial and time–spatial polarization separation. For this, the QWP is held in a computer-controlled rotating holder. The measurement first involves setting the orientation of the QWP fast axis to +45° to place the RHCP channel on the top track of the CCD and the LHCP on the bottom track. These first two polarization-encoded spectra are recorded. In a second step, the fast axis of the QWP is set to -45° to invert the polarization channels and the two polarization-encoded channels are recorded. This allows to measure the CPL along three ways:

**Spatial separation** : $I_L$ and $I_R$ simultaneous measured as the spectra coming from the two polarization encoded paths for one given QWP orientation (Figure 2-a);

**Time separation** : $I_L$ and $I_R$ successively measured on one optical paths for two QWP azimuth $\pm\frac{\pi}{4}$ (Figure 2-b);

**Spatial-Time combination** : $I_L$ (resp. $I_R$) is taken as the sum of the two left- (resp. right-) handed polarization measurements for the two QWP orientations (Figure 2-c).

## 2 Theoretical analyzis

### Principle

Ideally, all the configurations illustrated in Figure 2 lead to the same true CPL spectra. However, since the optical elements along the two paths and the pump source are not ideal, we must consider different experimental limitations. The detailed steps to obtain the intensity of the recorded light are given in the Supporting Informations. In here, we give only the major steps. Light is described using the 4-components of the Stokes

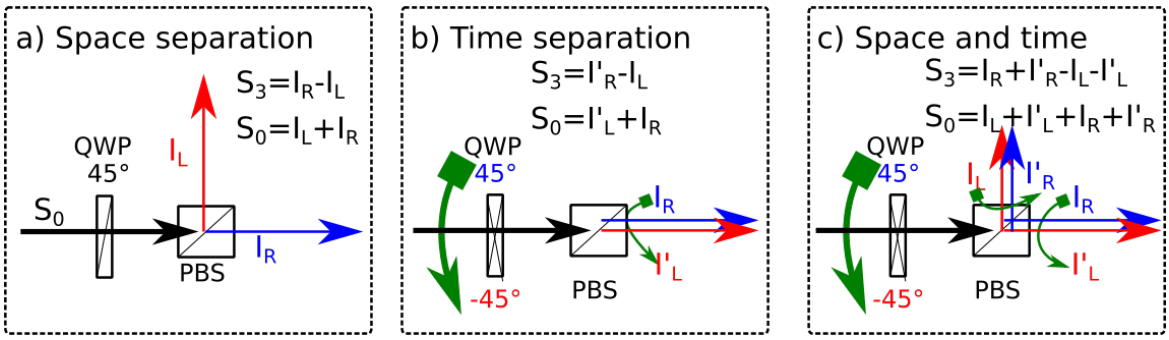


**Figure 2:** Three measurement's configurations to obtain CPL: Left and right circular polarisations encoded spectra are measured: (a) simultaneously through the two arms, (b) on the same arm after rotation of the QWP and (c) as the sum of the two previous ones.

| **Polarization separation** | **Signals combination** | **ZO** | **1$^{\mathbf{rst}}$ non null correction** | **False CPL signals** |
|---|---|---|---|---|
| Time: QWP (rotation) + PBS (One channel) | $I_{p,+1} - I_{p,-1}$ | $p(1-\epsilon_p)F_3S_3(\lambda)$ | $\Delta\phi S_0$ | Lum. |
| Spatial: QWP (fixed) + PBS (two channels) | $I_{+1,q} - I_{-1,q}$ | $q\eta_{mix}F_3S_3(\lambda)$ | $(\Delta T + \frac{\epsilon_+ - \epsilon_-}{2})S_0$<br>$\Delta\lambda\frac{\partial S_0}{\partial\lambda}$<br>$\eta_{mix}F_1S_1 + \eta_{mix}F_2S_2$ | Lum.<br>Lum. derivative<br>Linear Lum. |
| Time + Space | $(I_{1,1} - I_{-1,1}) -$<br>$(I_{1,-1} - I_{-1,-1})$ | $\eta_{mix}F_3S_3(\lambda)$ | $\eta_{mix}(\Delta\phi\Delta T + \frac{\epsilon_- \epsilon_-}{2})S_0$<br>$\eta_{mix}\Delta\phi\Delta\lambda\frac{\partial S_0}{\partial\lambda}$<br>$\eta_{mix}\Delta\phi(F_1S_1 + F_2S_2)$ | Lum.<br>Lum. derivative<br>Linear Lum. |

**Table 2:** CPL calculated at different orders of the experimental limitations using Equation 2 for three signal combinations. ZO is the result at zero order. First non nul order terms are in fourth column. The last column shows the corresponding unwanted spectral signals present in the main signal.

vector which are: the total intensity $S_0 = I_L + I_R$, the difference between the circularly polarized intensities $S_3 = I_R - I_L$ (opposite to the CPL) and the differences between the linearly polarized intensities $S_1 = I_{0°} - I_{90°}$ and $S_2 = I_{45°} - I_{-45°}$. References axes (0° and 90°) are chosen identical to the PBS ones.

Using the Mueller matrices of the different elements encountered along the optical paths, the Stokes vector at the detector can be derived as the product of the different Mueller matrices $\mathbf{M_i}$ representing each optical element:

$$\prod_i \mathbf{M_i} \cdot \mathbf{S}(\lambda) \tag{1}$$

where $\mathbf{S}(\lambda)$ is the Stokes vector of the emitted light.

We have calculated the four signals corresponding to the top and bottom arms measured twice with the QWP azimuth at $+\frac{\pi}{4}$ and at $-\frac{\pi}{4}$. Different experimental limitations have been taken into account: QWP phase retardation $\Psi \neq \pi/2$ and azimuth $\theta \neq \pm\pi/4$, unequal transmission of the two arms, spectral mismatch, cross-talk between the two arms and pump instability. Several reasons make the overall transmission of the two arms unequal: unbalance of the beamsplitter, unequal launching into the fibers, non-equal polarization response of the grating, ... We have gathered all these imperfections in a transmission factor called $T_{\pm1}$ for the top/bottom arms.

It is also important to consider the potential wavelength mismatch between the two spectra recorded simultaneously. It may come from a mis-alignement between the grating, the entrance slit and the CCD pixel matrix and induces that the two intensities recorded on the same vertical channel of the CCD correspond to the two sligthly different wavelengths $\lambda_{\pm1}$ for the top/bottom arms.

PBS imperfections, as well as straylight inside the monochromator, induce cross-talk between the two polarization encoded channels: a small relative part of one polarization falls into the detection area of the other one's. $\varepsilon_{+,-}$ denote the PBS inverse rejection rates and we assume that the straylight mixes a fraction $\sigma_l$ from one chanel to the other one's.

Finally, because we measure spectra at two different times, a possible drift of the pump source may occur. We model this pump instability as two exciting ratio $\phi_{\pm 1}$ for the $\pm\frac{\pi}{4}$ QWP azimuth orientation. All these sources with their quantification parameters are gathered in Table 1 and the corresponding Mueller matrices are described in SI section 5.

Taking into account all these effects, the spectra recorded for each arm following the two QWP azimuth orientations, write at first order:

$$I_{p,q} = \frac{\phi_q T_p}{2}\Big[(1+\epsilon_p)S_0 + p(1-\epsilon_p)(F_1 S_1 + F_2 S_2) + pq(1-\epsilon_p)F_3 S_3)\Big](\lambda + p\Delta\lambda) \tag{2}$$

where the subscript $p = \pm 1$ denotes the polarization channel after the PBS (+ and - for the horizontal and vertical polarization respectively) and the subscript $q = \pm 1$ denotes the orientations of the QWP fast axis ($\pm$ for $\pm\pi/4$) and therefore the pumping efficiency $\phi_{\pm 1}$ corresponding to the pump efficiency at the time of the measurements. The $F_i$ coefficents take into account the departure of the polarization elements from the ideal case:

$$F_1 = \sin^2 2\alpha - \cos^2 2\alpha \sin\psi \approx -\psi \ll 1 \tag{3}$$

$$F_2 = -\sin 2\alpha \cos 2\alpha(1+\sin\psi) \approx -2\alpha \ll 1 \tag{4}$$

$$F_3 = -\cos\psi\cos(2\alpha) \approx 1 \tag{5}$$

For each of the three configurations, combining equation 2 with the respective $(q,p)$ measurements pairs allows to derive the experimental luminescence (by summation) and CPL spectra (by differentiation) (SI sections 4.4-7). These calculations are performed as a power development with $S_0 \gg S_{i\neq 0}$ and the experimental defects taken a small first order effect (i.e. $\Delta T$, $\Delta\phi$, $\Delta\lambda\partial/\partial\lambda$, $F_1$ and $F_2 \ll 1$). The results are gathered in Table 2 for the CPL, the luminescence is given in the SI. In Table 2, the measured signals are ordered following the zero and the first non null terms of the power development.

As expected, the zero order corresponds to the expected signals, i.e. CPL to the nearest $\eta_{mix}F_3$ factor where $F_3$ denotes the QWP imperfection and :

$$\eta_{mix} = 1 - \frac{\epsilon_+ + \epsilon_-}{2} - 2\sigma_l \tag{6}$$

quantifies the reduction of the CPL coming from the mixing between the two arms. The higher order terms come from the experimental limitations that introduce unwanted signals which mix with the good one's. First order term in the luminescence signals are generally much smaller than the luminescence as they imply the product of the small CPL and linear birefringence signals modulated by the instrumental defects. We can therefore, safely assume that the sum signals are the luminescence ones'.

**Trueness of the CPL** At first order, the measured CPL is scaled down by two factors: $F_3$ coming from the QWP imperfections and $(1-\epsilon_p)$ or $\eta_{mix}$ for the time and spatial separation schemes respectively. As a product of cosinus of small angles (see Table 1), the $F_3$ coefficient is very close to one. With usual alignment procedures between to cross polarizers, $F_3$ may be keep higher than 0.99 on a 400nm range with standard achromatic QWP. CPL reduction coming from the PBS is about 1% and we measure in our home made monochromator a stray light coefficient lower than 4% over the whole spectral range. It gives an overall reduction factor of 0.95 on the measured CPL. The wavelength dependance of this factor is very smooth as it can be seen from retardance and rejection rate specifications given by different suppliers. Our own measurements one rejection rates and stray light validate this assumption (see SI Fig. 2). Therefore, we do not take into account this correction in the rest of the paper.

**Time separation of the polarizations** is presented in the first row of Table 2. It induces a false CPL signal ($\Delta\phi S_0$) coming from the variation of the excitation source between the two $I_L$ and $I_R$ measurements. Indeed, a pump variation between the two measurements cannot be discriminated from a true variation of $I_L$ with respect to $I_R$. This signal having the spectral shape of the luminescence can lead to erroneous interpretation. It cannot be subtracted as a baseline because, it is carried on by the signal itself. Therefore, designing a CPL apparatus requires that this first order term is negligible compared to $S_3$. As $S_3 = g_{lum}S_0$, we obtain the requirement on the pump stability to get CPL free from first order artifacts:

$$\Delta\Phi \ll g_{lum} \tag{7}$$

Practically, it means that for standard $g_{lum} \approx 10^{-3}$ the measurement of CPL by temporally inverting the polarization requires stabilized excitation sources with relative variation $\Delta\phi \leq 10^{-4}$. As the weakness of the CPL is the need for long integration time, it is practically impossible to avoid the excitation source variation except for the fast modulation techniques. Indeed, PEM modulation allows to invert the polarization selection at a very short time (a few µs) preventing any pump drift. Moreover, averaging over a large number of cycles increases the signal to noise ratio.

**Spatial separation of the polarization** is presented in the second row of Table 2. Simultaneous measurement over two polarization encoded paths completely remove the pump variation effects but three other artifacts appear. The first one ($\sim S_0$) is related to the non equal transmission between the two optical paths that can not be differentiate from a true non equal $I_L$ over $I_R$ luminescence. Less intuitive, the wavelength mismatch of the two recorded spectra induces a CPL signal proportional to the luminescence derivative ($\frac{\partial S_0}{\partial \lambda}$). QWP imperfections mix the linear luminescence into the CPL. The non-perfect retardance ($\psi$) couples with $S_1$ (0–90° polarization excess). This signal may appear in solid samples and also in solutions due to the polarization selectivity of the excitation light, for a 90° excitation/detection scheme. The wrong alignment of the QWP azimuth induces a coupling with $S_2$ (±45 linear polarization excess) and should be only relevant for anisotropic solid state samples. Because we work only with solution, we neglect these linear anisotropy terms in the following.

It is important to emphasize, that the artifacts described here are carried on by the fluorescence signal itself ($S_0$ and $\frac{\partial S_0}{\partial \lambda}$). They are not unwanted background and can not be simply substracted from a recorded spectra. Therefore, they add ambiguous contributions to the CPL with spectral feature having similar shapes as the CPL itself.

As $\frac{\partial S_0}{\partial \lambda} \approx S_0/\delta\lambda$ where $\delta\lambda$ is the luminescence spectral width, the requirements for the experimental parameters in order to get signal artifacts lower than x% of $g_{lum}$ are:

$$\Delta T \leq x\% \cdot g_{lum} \text{ and } \quad \Delta\lambda \leq x\% \cdot g_{lum} \cdot \delta\lambda \tag{8}$$

For example, at $10\% g_{lum}$ with small organic molecules ($g_{lum} \sim 10^{-3}$ and $\delta\lambda \sim$50nm), we get $\Delta T \leq 10^{-4}$ and $\Delta\lambda \leq 0.005$nm. For a higher $g_{lum} \sim 10^{-2}$ obtained for rare earth complexes ($\delta\lambda \sim 1$nm), the constraints are $\Delta T \leq 10^{-3}$ and $\Delta\lambda \leq 10^{-3}$nm. Whatever the kind of sample to measure, the required properties of the optical instruments (control of the transmissions better than 0.1%) and the need for monochromators with sampling steps lower than 0.001nm are unrealistic and could explain the discrepancies observed between the measurements made by camera and PEM-based set-ups for narrow lines rare-earth emitters[18]. A way to overcome this issue consists in a calibration procedure with a non polarized light. But, as the artifacts are proportional to the shape of the luminescence of the studied molecules, these calibration must be done with a racemic mixture of the molecule at the very same concentration. Our own practice showed us that these calibrations are very difficult to perform and must be re-evaluated almost before every measurement to be effective.

**Combination of time and spatial configurations** allows to reduce dramatically the artifacts related to the CPL measurement by our setup. Inspection of the first two rows of the Table 2 reveals that the first order terms do not depend on the $p$, $q$ parameters while CPL does. Consequently, artifacts add or subtract to the CPL depending on the two measuring schemes. Therefore, by adding the two CPL signals measured for the two configurations (last row of Table 2), the first order terms are canceled and the main remaining artifacts are products of $\Delta\phi$ with $\Delta T$ or $\Delta\lambda$ (see SI section 4.7 for the detailed calculation). The requirements to avoid false CPL are then:

$$\Delta\Phi\Delta T \leq x\% \cdot g_{lum}, \quad \Delta\Phi\Delta\lambda \leq x\% \cdot g_{lum} \cdot \delta\lambda \tag{9}$$

If spatial or temporal constraints alone are very difficult to maintain at very low level, the combination of spatial and temporal polarizations separations strongly reduces the effect of these constraints, rendering the experimental setup much easier to perform and thus reliable CPL measurements much easier to obtain.

A final important point is that the arm inversion must be done without changing the polarization before the monochromator. Indeed, gratings are very sensitive to the polarization with complicated wavelength dependence. Therefore, inserting rotating polarizers in front of the monochromator will mix arm mis-balance with monochromator polarization sensitivity. This is why we use the QWP before a PBS in such a way that the polarizations are unchanged on each detecting arm.

# 3 Experimental validation

## 3.1 Molecules and their fluorescence and CPL spectra

Two kind of molecular species have been used for this study : Camphorequinone **1**, a small organic molecule with broad emission band (reference molecule used by the CPL spectrometer manufacturer: JASCO [24]) and rare earth chiral complexes with narrow emission lines in order to put into evidence the CPL artifacts related to fluorescence and fluorescence derivative.

**1** have been purchased from TCI company in enantiopure form, 1(R)-(-)-Camphorequinone and 1(S)-(+)-Camphorequinone (SI, Figure 4). Fluorescence and CPL measurements have been carried out on solution samples by dissolving these molecules in ethanol. Typical concentration of $8.10^{-3}$mol.l$^{-1}$ were prepared.

Complexes **2** and **3** are isostructural complexes of $Eu^{3+}$ (**2**) and $Yb^{3+}$ (**3**), respectively. They were prepared in their enantiopure forms ([Ln**(R,R)-L**$_3$](OTf)$_3$ and [Ln**(S,S)-L**$_3$](OTf)$_3$), according to the procedure we previously described[21]. Their structures (see SI, Figure 4) was shown identical in both solid state and solution and their high brightness make them good candidates as a reference for the calibration of CPL set-ups.

For the measurements of **1**, with $g_{lum} \sim 10^{-2}$, we used a 830gr/mm grating leading to a dispersion over a 300 nm spectral range and a wavelength sampling interval of $\sim$ 0.3nm, at the CCD side. The resolution was 1nm and the integration time to get the presented spectra was 10minutes (5min for the acquisition of each configuration plus 10s time to rotate the QWP). Camphorequinone solutions were excited with an Laser diode (10 mW, $\lambda = 405$nm. The luminescence and CPL spectra displayed in Figure 3), present a broad single band extending from 400 to 550nm. To compare the spectra features are also recorded with our step by step setup using a standard PEM plus analyser system to differentiate via a lock-in amplifier the LHCP and RHCP. In this case, the spectral resolution was 1nm, the step was 0.25nm and the integration time was 7s/step. Spectra recorded with the two systems and corrected from the wavelength response, are very similar. The slight difference in the relative intensities of the fluorescence and CPL bands show the residual errors effects which are more visible in the case of wide emission bands, due to the different spectral response of the two setups. As for each of them, the error on the fluorescence and CPL measurements is the same, it is cancelled in the $g_{lum}$ spectra, as can be seen in Figure 3. It took two hours for the PEM-based setup against 10 minutes for the CCD-based one, to get spectra with equivalent signal to noise ratio.

For the measurements of complexes **2**, a (830gr/mm) grating was used with a twice optical magnification providing a spectral range and a wavelength sampling of $\sim$ 135nm and $\sim$ 0.15nm, respectively. Spectra were acquired under UV LED (4mW, $\lambda = 365$nm), with an equivalent resolution of 0.5nm and acquisition time of 10s for each spectrum at the CCD side and 2.1s/step at the PEM one. The measured fluorescence and CPL spectra display the usual features of $Eu^{3+}$ with 3 main lines in the visible part of the spectrum (Figure 4). Measurements using either the CCD (red line) or the step by step PEM (black circles) set-ups, give the same results as expected. The acquisition time for the CCD setup is 30s (10s for the acquisition of each configuration plus 10s time to rotate the QWP) against $\sim$20min for the monochanel system, to measure equivalent spectra

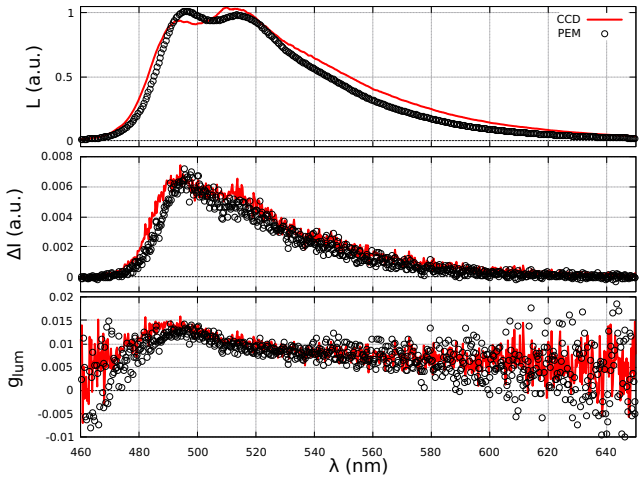


**Figure 3:** Luminescence (top), CPL (middle) and $g_{lum}$ (bottom) of **1** under 450 nm excitation. The scales luminescence and CPL are normalized to the maximum of emission. In red the spectra recorded with the CCD camera using the four signals procedure, in black circle the spectra recorded in a step by step set-up using a PEM+analyser system. Wavelength response correction has been applied for each system.

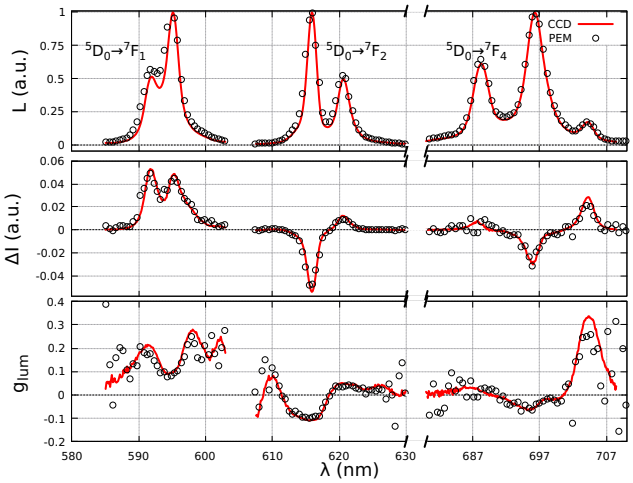


**Figure 4:** Three main visible transitions (luminescence (top), CPL (middle) and $g_{lum}$ (bottom)) of $Eu^{3+}$ complex **2** under 365nm excitation. In red the spectra recorded with the CCD camera using the time-spatial combination, in black circle the spectra are recorded in a step by step set-up using a PEM+Analyser system. The scales of each luminescence and CPL transitions are normalized to the maximum of emission.

with $g_{lum}$ of few $10^{-1}$.

## 3.2 CPL artifacts

In order to characterize the measurements artifacts with the CCD-based set-up we proceed as follow. we first, align our setup as well as possible. We take great care to make the two sensing paths as identical as can be (same lenses, same relative position of the optical elements, top and bottom tracks centered on the camera). The spectrometer is also precisely aligned: slit, grating and camera being parallel to each other, within one pixel. After that, we measure the CPL spectra according to our spatial-time procedure (red line curves in Figure 5). Then, we take off the quarter wave-plate and record exactly the same spectra. Assuming no linear fluorescence effects, we must get a zero CPL signal. However, because of the geometrical and spatial imperfections described in the theoretical part, non zero signal can arise. Mathematically speaking, taking off the QWP makes the $\mathbf{Q_q}$ (SI Eq. 3) equal to identity matrice. Therefore, $F_3$=$F_2$ = 0 and because $S_1 = 0$ (no linear dicroism) only the $S_0$ term remains and the recording signals are the artifacts listed in Table 2 ($4^{\text{th}}$ column).

Figure 5 displays the CPL artifacts measured on **1** and **2**. The difference between the two optical paths without QWP, result in the green curve showing a false CPL similar to the luminescence spectra of **1** whose intensity is of about 2.5% that of the luminescence spectra (Figure 3). This is the optical unbalance of our setup. For the $Eu^{3+}$ complex, the recorded signal present a false CPL opposite to the good one with an intensity of 7% of the luminescence (Figure 4). This 2.5-7% of intensity variation is the optical limitation for the spatial separated polarizations-based set-ups and only CPL with $g_{lum} \gg 0.05$ can be safely measured. The stability of the excitation source is given by the differential measurement on the same channel but at 20s interval (blue curve). Depending on the source, high power laser for **1** or low power light emitting diode for **2**, we observe intensity variation of about 1% and 0.5% respectively. This is the limitation of time separated polarizations-based set-ups. Finally, as described in the theoretical part, the combination of four measurements (black curve) through the time-spatial-based configuration dramatically decreases the artifacts down to $10^{-4}$ as the product of 2.5-7% times 0.5-1%. It allows the safe study of samples with $g_{lum} \geq 10^{-3}$.

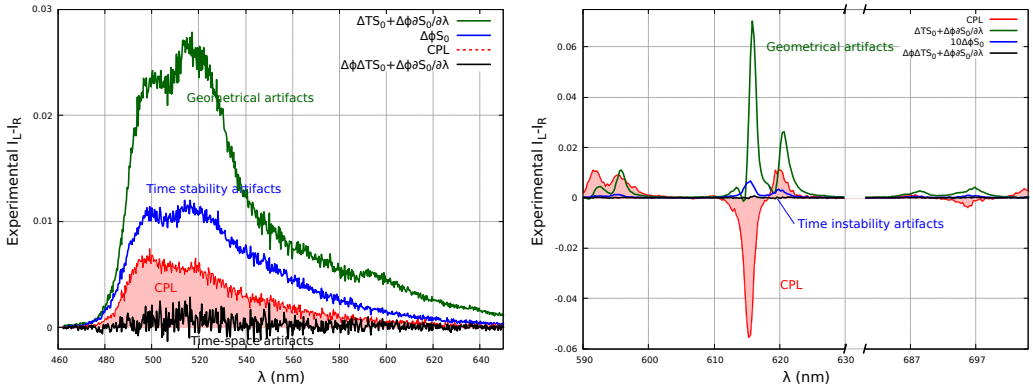


**Figure 5:** CPL artifacts of **1** (left) and **2** (right) recorded without the QWP (green -blue and black). To compare the CPL measured by the four signals combination is plotted in red. **1** is excited with a $\lambda$ =365 nm emitting diode with 2 s integration time. **2** is excited with a $\lambda$ =450 nm laser with 15 s integration time. Signals are normalized by the maximum of the luminescence. The green curves are the signal difference between the two polarization encoded arms: it images the unbalance of the optical paths. In blue, the signal difference for two measurements delayed by 20s obtained on the same arm, this is the the $\Delta\phi$ light source relative variation. 20s represents the required time to rotate the QWP by 90°. Black curves result from spatial-time combination.

## 3.3 Robustness

Here, we experimentally investigate the robustness of the artifact-free CPL procedure. Starting from our best aligned setup, we degrade on purpose some parts and record the corresponding spectra.

**Transmission misbalance** We place a variable neutral density filter in front of one of the two lenses $L_2$ (see optical setup figure 1), in order to lower the transmission along one polarization encoding path. The recorded CPL spectra are displayed in Figure 6 for **1** (left) and **2** (right). The measured CPL spectra using the four signals configuration are completely insensitive to the transmission difference between the two arms in the investigated range up to $\Delta T = 0.1$ for **1** and $\Delta T = 0.4$ for **2**.

To compare, the CPL obtained for the spatial separated polarization are also displayed in the bottom panels. By looking at the luminescence spectra (Figure. 3-4), the CPL artifacts clearly depends on the luminescence as described by the term $\Delta T \times S_0$ (Table 2). On the bottom left of the figure, the false measurement are

nearly proportional to $\Delta T$ with a shape very similar to the luminescence spectra of the corresponding molecule (Figure. 3) with some ripple effects attributed to the slow wavelength dependence of $\Delta T$. On the bottom right, the narrow emission lines only let appear the shape of the luminescence in the false CPL.

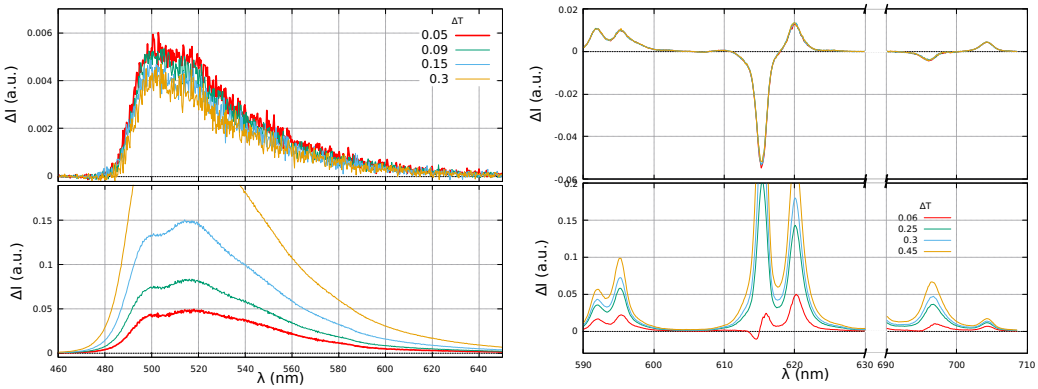


**Figure 6:** CPL of **1** (left) and **2** (right) by using either the artifacts-free procedure (top) or taking one single $I_L$-$I_R$ difference (bottom). Note the y-axis different range between the top ans bottom. The different curves are recorded for different neutral density attenuation on one arm. The average transmission difference factor $< \Delta T >$ is calculated from the luminescence integral measured at each arm.

**Wavelength mismatch** To add a small wavelength mismatch between the two polarization encoded spectra, we tilt a bit the camera away from the well aligned position. Again, we show that there is not any difference in the recorded CPL spectra using the time-spatial procedure (top spectra of Figure. 7). For this experimental mis-alignement, the CPL artifacts present in the spatial separated polarization procedure are related to the fluorescence derivative as illustrated in the bottom part of Figure. 7. The order of magnitude of the measured CPL compare to the luminescence derivative for the Eu complex (right bottom), shows that for our best set-up (red curve) the wavelength mismatch is negligible around 595nm and is about 0.02 nm and 0.1 nm at 620 and 700 nm respectively. It indicates that, under best alignment, we can not guarantee a perfect spectral matching on the whole spectral range (here 120 nm). Moreover, as the spectral sampling interval is 0.13 nm, it is not possible to get a better accuracy and the CPL artefact related to this wavelength mismatch between the two recorded spectra on two different part of the CCD is inevitable. However, our procedure is very stable in term of CPL results with reproducible spectra even with strong misalignment (see the image distortion obtained for a 1.6° tilt in the SI section 6).

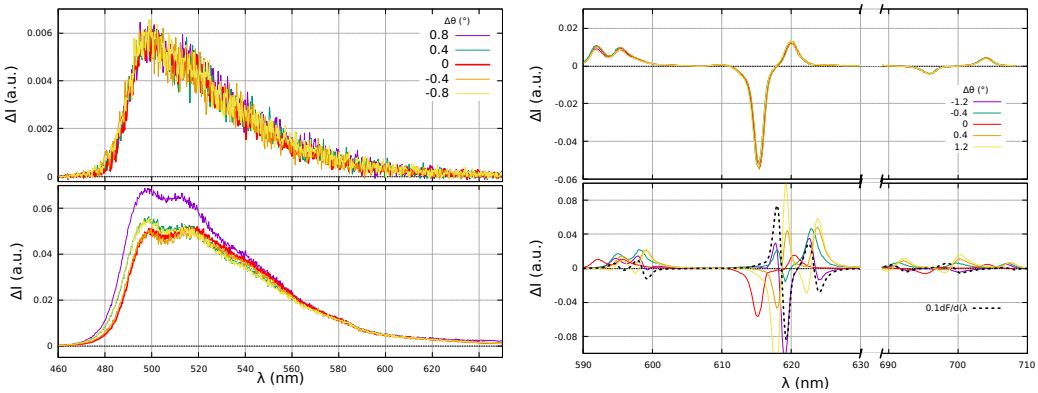


**Figure 7:** CPL of **1** (left) and **2** (right) by using either the artifacts-free procedure (top) or taking one single $I_L$-$I_R$ difference (bottom). The different curves are recorded for differents tilt mis-alignement of the CCD camera. Note the y-axis scale difference between the top and bottom panels. The dashed black curves are the derivative of the luminescence signal.

## 3.4 Linearity

We prepare two enantiopure solutions of $Eu^{3+}$ complex **2** with the same concentration of ($10^{-5}$mol/l) but with opposite handedness. We record a series of CPL spectra starting from one enantiopure solution and by adding,

gradually, the opposite enantiopure solution to the first one, we decrease the CPL of the mixture gradually until it is cancelled for the racemic solution. The idea is to decrease the CPL signal gradually at a constant emission in order to characterize the linearity of the measurements. Figure. 8 clearly shows this gradual racemization effect and the decrease in intensity of the CPL, the inset in the figure attests for the linearity of our measurements.

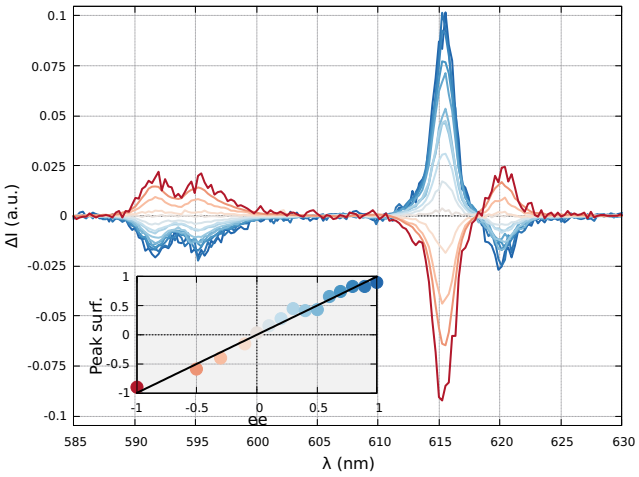


**Figure 8:** CPL spectra measured for different enantiomeric excess ee. The inset displays the surface of the 615nm peak versus ee.

## 3.5 Signal to noise ratio

The CPL spectra of **1** is displayed in Figure 9 for different integration times from 1s to 256s using the CCD apparatus (this is the integration time for one QWP configuration). As expected, the signal to noise ratio (SNR) increases with the integration time, and this without any artifacts coming from the lamp stability. To compare, we have used the same source and the same solution to record the CPL spectra with a step by step mono-chanel setup (PEM plus analyser). The overall experimental time of 480s (i.e. a step=2.5nm and an integration time= 2.1s/step ) results in the black dotted spectra plotted in the top of the figure. The SNR is similar to what is obtained with the camera for 1s integration time spectra. For similar wavelength sampling interval, same spectral range and a comparable SNR, the recording with the camera is ∼500 times faster.

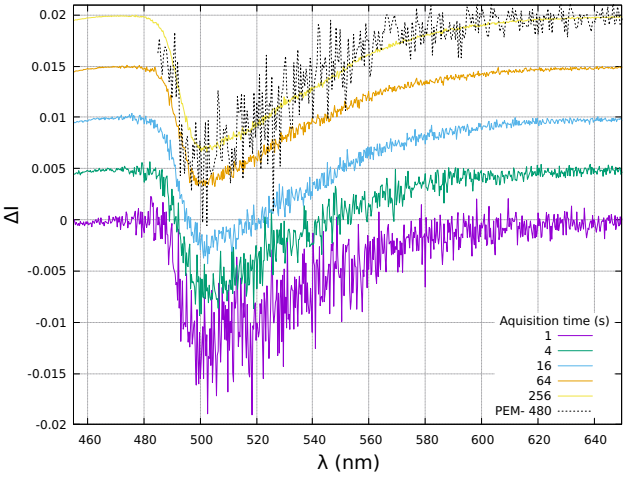


**Figure 9:** CPL spectra of camphorequinone excited with a $\lambda$ =450nm laser, recorded with the CCD spatial-time configuration at different integration times from 1-256s and the counterpart, in black-line, recorded with the step by step (PEM + analyser) based setup, with 1s/step integration time.

# 4 CPL in the near IR

Our setup can operate in a wide wavelength range from the UV to the near IR. Indeed, by changing only the PBS cube and the transmission grating, we can easily switch from the UV-visible to the near infrared spectral range. All other optical and detection elements (QWP, lenses, fibers and CCD) are chosen to cover the entire spectral range from 300 nm to 1.1 µm. Thereby, CPL of enantiopure complexes **3** ([$Yb^{3+}$**(R,R)-L**$_3$](OTf)$_3$ and [$Yb^{3+}$**(S,S)L**$_3$](OTf)$_3$) are recorded using the spatial-time procedure, for the two enantiomers and compared with their counterparts obtained by our single chanel PEM based setup with appropriate IR PM detector (Hamamatsu H10330B-75).

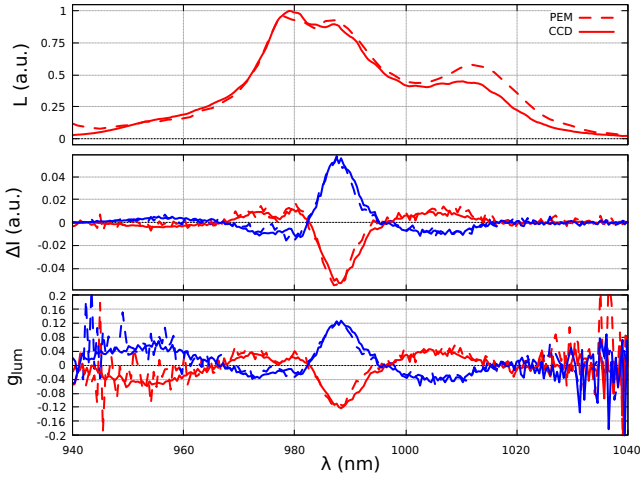


**Figure 10:** Luminescence (top), CPL (middle) and $g_{lum}$ (bottom) for the two enantiomers of **3** under 450nm excitation. The scales luminescence and CPL are normalized to the maximum of emission, so that the $g_{lum}$ value at maximum luminescence, can be directly read on the y-axis. In continuous line spectra recorded with the CCD camera using the spatial-time procedure, in dashed line the spectra recorded in a step by step mode using a PEM+analyser system. Wavelength response correction has been applied for each system.

The spectra are recorded over 940-1040nm spectral range, under 450nm laser excitation (power 10mW). The four obtained luminescence spectra are similar but to avoid crowding the graph, we only show on Figure 10, one emission spectra for one enantiomere, measured by each setup. The normalised emission spectra are almost identical and are typical of $Yb^{3+}$. The difference in intensity at long wavelengths, despite their correction by the spectral response of the corresponding setup, is due to the detection limit of the CCD in this spectral range, inducing a high error scale. The corresponding CPL bands are well mirror images for the two enantiomers and for each of them, the spectra obtained by both setups are identical in terms of number of bands, their shapes and their positions in wavelength as well as their relative intensities, as attested by Figure 10. Even though the $g_{lum}$ value of the measured $Yb^{3+}$-complexes is rather high ( $10^{-1}$), the measurement of the CPL on the PEM side is more time demanding because of the low signal to noise ratio of the detector in this wavelength range.

It took thus, 420s (step = 0.5nm/integration time = 2.1s/step) to record a CPL spectrum on the PEM side while only 0.1s per spectrum (i.e. a global time of 10.2s: 2 spectra + QWP rotation) was needed to obtain the same spectrum with, moreover, a better SNR, at the CCD side. Here again, our CCD-based setup with the spatial-time method shows its strength for the measurement of fast and reliable CPL in the near IR range. This range can be extended by the use of adapted CCD.

It is worth noting that to date, only a few pioneering works concerning the measurement of CPL in the near IR region, using the conventional CPL spectrometer, have been reported [21, 23, 25, 26]. IR region remains thus, a relatively new area to explore for CPL emitting materials and relative potential applications.

# 5 Discussion

The CPL measurement by combining four measures corresponding to spatial and temporal separation of the circular polarizations allows a self-compensation of the artifacts and the direct measurement of $S_3$ to the nearest $\eta_{mix}F_3$-factor (Table 2, third columns) with $F_3$ and $\eta_{mix}$ defined in Eq. 5-6.

$\eta_{mix}F_3$-**factor** : This corrective-factor reflects the deviation from the linearity of the system due to the QWP related errors and the polarization mixing in the two encoded optical paths (stray-light + PBS imperfection). These errors cannot be suppressed for any of the tree CPL measurements methods based on CCD . All we can do , is to minimize them as much as possible.

- QWP related errors: phase retardation $\Psi \neq \pi/2$ and azimuth $\theta \neq \pm\pi/4$ are taken into account by $\cos\psi$ and $\cos(2\alpha)$ (with $\psi = \Psi - \frac{\pi}{2}$ *and* $\alpha = \theta - \frac{\pi}{4}$), terms respectively. As these two corrective factors are *cosinus* dependent, their effects are minimal. Indeed, a phase delay $\Psi = \frac{\pi}{2} \pm \frac{\pi}{100}$ (standard specification of achromatic QWP over a few hundreds of nm) induces an error of 0.2% on the measured CPL. QWP azimuth accuracy around 0.1deg can be easily achieved using standard alignment procedure by placing the QWP between two cross polarizers. Even if this orientation is not accurate, a misalignment of $\pm 2°$ results in an error of 0.06%. Therefore, a standard quality of the QWP and its rough orientation does not induce significant errors on the CPL magnitude.

- Mixing polarization related errors, $\eta_{mix}$: contrary to the QWP, the quality of the PBS or of any polarizer used in a CPL measurement setup is very important. If the polarizer rejection ratio is 90%, for example, then 10% of one polarization is injected in the arm transporting the other one. This results in an underestimation of the CPL of 20%. Thus, the better the polarizer, the lower the error on CPL. Besides, a small relative part of one polarization falls into the detection area of the other one's depending on the straylight of the spectrometer. This leads again, to an underestimation of the CPL of 2 to 4% in our setup. The straylight is the limit of CPL measurements setups based on a single spectrometer. The use of two spectrometers improves this aspect but will introduce a new source of errors due to the responsivity drift between the two detectors.

**Artifacts sources** : the artifacts sources for the three configurations of CPL measurements, have been identified. The theoretical analysis of these artefacts show that their spectral shape is proportional to the fluorescence signal and to its derivatives and therefore, cannot be subtracted as a simple baseline. Besides, their experimental quantification, by taking off the QWP and measuring each of them, allow to asses the limits of each configuration.

- Artefacts related to the spatial separations of the polarization i.e. non equal transmission ($\Delta T S_0$) and wavelength mismatch ($\Delta\lambda\frac{\partial S_0}{\partial\lambda}$) between the two optical paths (Table 2, second column) can not be suppressed in the case of CPL measurements using only spatial separation. The constraints on $\Delta T$ and $\Delta\lambda$ are CPL dependent ($\Delta T \ll g_{lum}$ ; $\Delta\lambda \ll g_{lum}\cdot\delta\lambda$) and require unrealistic control of the transmissions, better than 0.1% and spectrometer sampling step, lower than 0.001nm. Experimentally, with the best alignment of our setup, the umbalance between the two arms induced not only false CPL whose intensity is about $2.5-7\%$ that of the luminescence, but also CPL band opposite to the good one, in the case of narrow emission bands (Figure 5). Indeed, the artifacts related to the wavelength detuning are proportional to the derivative of the luminescence signal and therefore more important for the narrow emission lines. They introduced false CPL signal with intensity of $\sim$ 8% that of the luminescence.

  Hence, in order to avoid as much as possible these false CPL contributions in the measured signal by only the spatial separation configuration, adapted and rigorous calibration, using racemic sample and non polarized light, is needed and have to be checked before each set of measurements.

- These constraints are no longer relevant in the case of CPL measurements by temporally inverting the polarization, as only one optical path is involved. However, to get non-erroneous CPL spectra, the excitation source stability is crucial with its variation between the two $I_L$ and $I_R$ measurements, $\Delta\Phi \ll g_{lum}$. This stability is difficult to ensure during the two successive measurements, especially since long integration times are necessary for accurate CPL measurements. Using a LED excitation source with long term stability of a few percents and standard optical elements, false CPL signal whose intensity is equal to 1% of the luminescence, was measured.

- By combining spatial and temporal-separation of the circular polarization and performing two sets of measurements where the role of the polarization encoded arms are inverted, then combining the four obtained measures, the first order artefacts relative to the two precedent configurations vanish and only second order terms remain, (see Table 2, third line). Apart from the CCD calibration for wavelength accuracy, fast CPL spectra can then be safely recorded by the CCD-based spectrophotometer without the need for tedious alignment and heavy calibration procedure each time a sample is changed or an optical element is moved.

Compared to the standard modulation technique with lock-in amplifier, CCD-based devices do not have AC filter. Therefore, the intensity resolution is the same over the whole range of the measurement and small signals are difficult to extract. In our case, with a 16 bits camera, the analog to digital conversion leads to an accuracy of $\frac{1}{2^{16}} = 1.5\ 10^{-5}$ for a full signal range. This is the fundamental lower limit for $g_{lum}$.

Finally, it is worth to remind here, that whatever the spectroscopic instrument used, it is necessary to take into account its wavelength response and to correct the measured spectra by the corresponding device function. Otherwise, the relative intensity of the spectral bands can be wrong. This remains a delicate operation if we want to compare measurements obtained by two different setups. Indeed, each spectrum must be corrected by the instrument function with which it was obtained and the instrument functions themselves, must be recorded properly. If we consider the spectra of Camphorequinone and $Yb^{3+}$-complexes, with large emission bands, (Figure 3 and Figure 10, respectively) we can see that, despite the wavelength response correction, there is still difference mainly in the relative intensities of the luminescence and CPL bands. However, as this error is the same on both measurements, it disappears in the $g_{lum}$ and there, we can really compare the two methods more safely.

# Conclusion

Measuring CPL is a delicate matter because it requires making a differential measurement with a relative precision of $10^{-5}$ on the emission signal. Therefore, the smallest artifacts can have a value of the same order of magnitude as the CPL itself or even larger leading to false CPL spectra. For this reason, modulation systems (PEM + lock-in amplifier) and a step by step measurements, with a very long integration time are generally used to extract the good signal.

In order to reduce the acquisition time and still obtain reliable spectra, a CPL spectrophotometer based on only one CCD camera and the combination of two inverted polarization encoded channels has been theoretically analyzed, set up and tested on two different classes of molecules giving narrow or broad band spectra respectively. We studied the limitations of three different configurations of this set up: time, spatial and spatial-time separations of the polarization.

We demonstrated that unless using a rigorous and heavy calibration procedure, the artifacts related to the two first configurations cannot be completely suppressed and thus, inevitably lead to more or less false CPL spectra. This can range from a wavelength shift, deformation, false relative intensities to a sign reversal of the CPL bands. Consequently, a misinterpretation of stereochemical structures and associated transitions of the studied chiral system or a wrong evaluation of the $g_{lum}$ is very likely. However, we showed that the third configuration, i.e. the spatial-time combination is the most efficient for obtaining reliable CPL spectra capable of measuring $g_{lum} > 10^{-4}$ in a robust, reproducible and fast way. It offers many advantages over CPL measurement by only time or only spatial separation of the polarization :

1. Accurate and fast measurement with standard optical elements for $g_{lum} \geq 10^{-3}$
2. Nearly no need for calibration, the measured signal is directly the CPL times a correcting factor $\in [0.92 - 1.00]$ coming mostly from the residual straylight and the PBS imperfections;
3. Auto-compensation of the artifacts at first order. The remaining artifacts are set at a very low value around $10^{-5}$ times the luminescence; No need of high quality QWP
4. Possibility to simply measure the artifacts on the *same sample* by just taking off the QWP.

Compared to a more standard mono-chanel setup with polarization modulation, the recorded time is reduced by three order of magnitude, for the same signal to noise ratio, and a fast measurement on a whole spectral range is obtained in one shot.

The implementation of such a fast and robust CPL spectrophotometer opens interesting perspectives for the monitoring of dynamic processes such as chemical reactions that vary over time, depending on a particular parameter. Moreover, thanks to its rapid measurements, the stabilization of the external parameter, such as temperature or magnetic field, is not any more as critical as in the case of much longer measurements with PEM-based setups.

Finally, this method can also be valuable for an automatic screening of enantioselective syntheses.

# References

[1] Prasad L. Polavarapu. *Chiroptical Spectroscopy:Fundamentals and Applications*. CRC Press, 2016. 1

[2] James P. Riehl and Frederick S. Richardson. Circularly polarized luminescence spectroscopy. *Chem. Rev.*, 86(1):1–16, February 1986. 1

[3] Hiroki Tanaka, Yoshihisa Inoue, and Tadashi Mori. Circularly polarized luminescence and circular dichroisms in small organic molecules: Correlation between excitation and emission dissymmetry factors. *ChemPhotoChem*, 2(5):386–402, May 2018. 1

[4] Lorenzo Arrico, Lorenzo Di Bari, and Francesco Zinna. Quantifying the overall efficiency of circularly polarized emitters. *Chemistry – A European Journal*, 27(9):2920–2934, 2021. 1

[5] Marcin Gorecki, Francesco Zinna, Tarita Biver, and Lorenzo Di Bari. Induced circularly polarized luminescence for revealing DNA binding with fluorescent dyes. *J. Pharm. Biomed. Anal.*, 144:6–11, Sep 2017. 1

[6] Yuki Imai, Yuka Nakano, Tsuyoshi Kawai, and Junpei Yuasa. A Smart Sensing Method for Object Identification Using Circularly Polarized Luminescence from Coordination-Driven Self-Assembly. *Angew. Chem.*, 130(29):9111–9116, 2018. 1

[7] Laure Guy, Maelle Mosser, Delphine Pitrat, Jean-Christophe Mulatier, Mercedes Kukułka, Monika Srebro-Hooper, Erwann Jeanneau, Amina Bensalah-Ledoux, Bruno Baguenard, and Stéphan Guy. Modulation of Chiroptical Properties in a Series of Helicene-like Compounds. *J. Org. Chem.*, 84(17):10870–10876, Sep 2019. 1, 2

[8] Francesco Zinna, Mariacecilia Pasini, Francesco Galeotti, Chiara Botta, Lorenzo Di Bari, and Umberto Giovanella. Design of lanthanide-based OLEDs with remarkable circularly polarized electroluminescence. *Adv. Funct. Mater.*, 27(1):1603719, 2017. 1

[9] Yongjing Deng, Mengzhu Wang, Yanling Zhuang, Shujuan Liu, Wei Huang, and Qiang Zhao. Circularly polarized luminescence from organic micro-/nano-structures. *Light: Science & Applications*, 10(1):76, April 2021. 1

[10] Jianmei Han, Song Guo, Hu Lu, Shujuan Liu, Qiang Zhao, and Wei Huang. Recent progress on circularly polarized luminescent materials for organic optoelectronic devices. *Advanced Optical Materials*, 6(17):1800538, 2018. 1

[11] Yadong Zhang, Shu Yu, Bing Han, Yunlong Zhou, Xiuwen Zhang, Xiaoqing Gao, and Zhiyong Tang. Circularly polarized luminescence in chiral materials. *Matter*, 5:837–875, 2022. 1

[12] Yuze Dong, Yupeng Zhang, Xinyue Li, Yaqing Feng, Han Zhang, and Jialiang Xu. Chiral perovskites: Promising materials toward next-generation optoelectronics. *Small*, 15(39):1902237, 2019. 1

[13] Katarzyna Staszak, Karolina Wieszczycka, Valentina Marturano, and Bartosz Tylkowski. Lanthanides complexes - chiral sensing of biomolecules. *Coordination Chemistry Reviews*, 397:76–90, October 2019. 1

[14] Takunori Harada and Kazusa Manabe. Chiroptical spectrophotometer and analytical method for optically anisotropic samples. *Rev. Sci. Instrum.*, 91(12):125108, December 2020. 1

[15] Carin R. Lightner, Daniel Gisler, Stefan A. Meyer, Hannah Niese, Robert C. Keitel, and David J. Norris. Measurement of raman optical activity with high-frequency polarization modulation. *J. Phys. Chem. A*, 125(36):8132–8139, September 2021. 1

[16] Oriol Arteaga, Zoubir El-Hachemi, Adolf Canillas, and Josep Maria Ribó. Transmission mueller matrix ellipsometry of chirality switching phenomena. *Thin Solid Films*, 519(9):2617 – 2623, 2011. 5th International Conference on Spectroscopic Ellipsometry (ICSE-V). 2

[17] Werner Hug and Gilbert Hangartner. A novel high-throughput raman spectrometer for polarization difference measurements. *J. Raman Spectrosc.*, 30:841–852, 1999. 2

[18] Lewis E. MacKenzie, Lars-Olof Pålsson, David Parker, Andrew Beeby, and Robert Pal. Rapid time-resolved circular polarization luminescence (cpl) emission spectroscopy. *Nat. Commun.*, 11(1):1676, April 2020. 2, 3, 6

[19] Frawley Andrew T., Pal Robert, and Parker David. Very bright, enantiopure europium(iii) complexes allow time-gated chiral contrast imaging. *Chem. Commun.*, pages 13349–13352. 2, 3

[20] Bruno Baguenard, Amina Bensalah-Ledoux, Cyprien Gindre, Stephan Guy, Laure Guy, Olivier Maury, Francois Riobe, Claudia Lalli, Carlo A. Mattei, and Fabrice Pointillart. Fast circularly polarized luminescence (cpl) spectroscopy. *31th International Symposium on Chirality -CHIRALITY 2019 14-17 July 2019, (Bordeaux, France)*. 2

[21] Frederic Gendron, Sebastiano Di Pietro, Laura Abad Galan, Francois Riobe, Virginie Placide, Laure Guy, Francesco Zinna, Lorenzo Di Bari, Amina Bensalah-Ledoux, Yannick Guyot, Guillaume Pilet, Fabrice Pointillart, Bruno Baguenard, Stephan Guy, Olivier Cador, Olivier Maury, and Boris Le Guennic. Luminescence, chiroptical, magnetic and ab initio crystal-field characterizations of an enantiopure helicoidal yb(iii) complex. *Inorg. Chem. Front.*, 8:914–926, 2021. 2, 7, 12

[22] Carlo Andrea Mattei, Kais Dhbaibi, Bertrand Lefeuvre, Vincent Dorcet, Gilles Argouarch, Olivier Cador, Boris Le Guennic, Olivier Maury, Claudia Lalli, Stéphan Guy, Amina Bensalah-Ledoux, François Riobé, Bruno Baguenard, and Fabrice Pointillart. Circularly polarized luminescence of eu(iii) complexes with chiral 1,1'-bi-2-naphtol-derived bisphosphate ligands. *Chirality*, 34(1):34–47, 2022. 2

[23] Bertrand Lefeuvre, Carlo Andrea Mattei, Jessica Flores Gonzalez, Frédéric Gendron, Vincent Dorcet, François Riobé, Claudia Lalli, Boris Le Guennic, Olivier Cador, Olivier Maury, Stéphan Guy, Amina Bensalah-Ledoux, Bruno Baguenard, and Fabrice Pointillart. Solid-state near-infrared circularly polarized luminescence from chiral ybiii-single-molecule magnet. *Chemistry - A European Journal*, 27(n/a):1, 2021. 2, 12

[24] JASCO. *https://jascoinc.com/applications/cpl-measurement-camphorquinone-using-cpl-300-circularly-polarized-luminescence-spectrometer/*, consulted Mars 2022. 7

[25] Francesco Zinna, Lorenzo Arrico, and Lorenzo Di Bari. Near-infrared circularly polarized luminescence from chiral yb(iii)-diketonates. *Chem. Commun.*, 55:6607–6609, 2019. 12

[26] Christine L. Maupin, David Parker, J. A. Gareth Williams, and James P. Riehl. Circularly polarized luminescence from chiral octadentate complexes of yb(iii) in the near-infrared. *Journal of the American Chemical Society*, 120(40):10563–10564, 1998. 12

## Supplementary Files

This is a list of supplementary files associated with this preprint. Click to download.

- SIStokesMueller.pdf